Nova Southeastern University
NSUWorks

Oceanography Faculty Articles

Department of Marine and Environmental Sciences

3-15-2001

An Approach to Parameterization of the Oceanic Turbulent Boundary Layer in the Western Pacific Warm Pool

Alexander Soloviev
Nova Southeastern University, soloviev@nova.edu

Roger Lukas
University of Hawaii at Manoa

Peter Hacker
University of Hawaii at Manoa

Find out more information about Nova Southeastern University and the Oceanographic Center.

Follow this and additional works at: http://nsuworks.nova.edu/occ_facarticles

Part of the Marine Biology Commons, and the Oceanography and Atmospheric Sciences and Meteorology Commons

NSUWorks Citation

An approach to parameterization of the oceanic turbulent boundary layer in the western Pacific warm pool

Alexander Soloviev

Oceanographic Center, Nova Southeastern University, Dania Beach, Florida

Roger Lukas and Peter Hacker

School of Ocean and Earth Science and Technology, University of Hawaii, Honolulu

Abstract. Vertical profiles of zonal velocity and the dissipation rate ε of the turbulent kinetic energy obtained during the Tropical Ocean-Global Atmosphere Coupled Ocean-Atmosphere Response Experiment (COARE) are analyzed in the context of planetary boundary layer relationships previously derived from atmospheric measurements. The presence of a barrier layer and the striking effect of increased dimensionless shear and ε at the bottom of the surface mixed layer of the ocean, features often observed in the western Pacific warm pool area, are consistent with the boundary layer laws. The gradient Richardson number Ri is found to be a convenient parameter for scaling the nonstationary and horizontally heterogeneous mixed layer in the warm pool area. The approach to parameterization of the turbulent eddy coefficient within the mixed layer as a function of Ri is tested as part of a one-dimensional model. A comparison between the observed and modeled upper ocean temperatures for two COARE examples shows a reasonable agreement over a wide range of wind speed conditions.

1. Introduction

The surface turbulent boundary layer of the ocean is an essential element of the general ocean circulation in the equatorial region [*Robinson*, 1960; *Moore and Philander*, 1977; *McCreary*, 1981]. Modeling of the equatorial warm pools, which are climatically important regions of the world ocean [*Webster and Lukas*, 1992], substantially depends on the mixing parameterization scheme. Although the planetary turbulent boundary layer has been intensively studied both in the atmosphere and ocean, the parameterization of vertical mixing in the upper ocean is still a challenge [*Pacanowski and Philander*, 1981; *Peters et al.*, 1988; *Yu and Schopf*, 1997].

The surface layer of the ocean is subject to strong turbulent mixing; the turbulence and the turbulent exchange coefficients are much higher than those below this region. This layer is also called the mixed layer since temperature and salinity are often observed to be vertically uniform near the surface. Although temperature, salinity, and shear gradients within the mixed layer are small (and relatively difficult to measure), they are associated with such dynamically important processes as the vertical buoyancy and momentum fluxes.

In the literature, both terms, the surface turbulent boundary layer and the mixed layer of the ocean, have been used interchangeably. In this paper, however, we will reserve the former term (surface turbulent boundary layer) for the layer with active turbulent mixing; while the latter term (mixed layer) will be used for the layer that has been mixed but may be no longer actively mixing. Note that the mixed layer depth defined from the density criteria does not necessarily coincide

with the turbulent boundary layer depth defined from turbulence criteria.

The effect of stratification on the turbulent boundary layer can be characterized via the stability parameter, $\zeta = z/L_O$, where z is the depth and L_O is the Oboukhov length scale $(L_O = u_{*_0}^3/(\kappa B_0))$, where B_0 is the surface buoyancy flux, u_{*_0} is the surface friction velocity, and $\kappa \approx 0.4$ is the Karman's constant). Another parameter related to stratification effects in the turbulent boundary layer is the gradient Richardson number defined as [see e.g., *Mellor*, 1996],

$$Ri = \frac{g\rho^{-1}\partial\rho/\partial z}{(\partial u/\partial z)^2 + (\partial v/\partial z)^2}, \quad (1)$$

where ρ is the density, z is the depth, u and v are the horizontal velocity components, and g is the acceleration of gravity.

Although ζ and Ri are both related to the stratified turbulent boundary layer, ζ is a function of the boundary conditions and Ri is a function of the local density and velocity gradients. For the stationary turbulent boundary layer, parameters ζ and Ri are interrelated (see section 3.1). For nonstationary conditions the surface layer of the ocean acts as a low-pass filter with respect to the variable heat flux at the air-sea interface. The thermal response of the upper ocean in the warm pool area is of the order of $t_T \sim 3$ days [*Lagerloef et al.*, 1998]. As a result, the information about changes in ζ, the parameter containing the surface heat and momentum flux, propagates within the mixed layer on this timescale. This makes it difficult to use the stability parameter ζ for scaling nonstationary turbulent boundary layers. At the same time the local gradient characteristics of the flow (constituting the Richardson number Ri) equilibrate on the timescale of turbulent dissipation t_ε, which is of the order of several tens of minutes at maximum [*Zil-*

itinkevich et al., 1978]. *Ri* rather than ζ is therefore the relevant parameter for scaling the nonstationary and horizontally heterogeneous surface mixed layer in the warm pool area.

The turbulent boundary layer depth *h* can be defined from the Richardson number criteria, $Ri = Ri_{cr}$. Above the critical value of *Ri* (thought to be 0.20-0.25), turbulence levels are small.

At *Ri* < 0 the flow is convectively unstable and turbulent mixing intensifies; as *Ri* becomes more negative, the turbulent eddy coefficient K_x increases [*Mellor*, 1996]. Neutral flow corresponds to *Ri* = 0. In the range -0.1 < *Ri* < 0.05 the influence of stratification is negligible and *Ri* falls out from the set of determining parameters; in these conditions the so-called logarithmic layer develops.

Ri-type mixing schemes have been employed in several parameterization and modeling studies, both in the atmosphere [see *Monin and Yaglom*, 1971] and ocean [*Pacanowski and Philander*, 1981; *Price et al.*, 1986; *Peters et al.*, 1988; *Yu and Schopf*, 1997; *Soloviev et al.*, 1999]. For the surface turbulent boundary layer of the ocean the direct verification of such parameterizations has, however, been complicated by the errors of velocity measurements. Within the turbulent bound-

ary layer the observed shear is usually small (of the order of value of the measurement accuracy or even less), which results in an enormous relative error of the Richardson number calculation. (Note that in (1) the shear enters into the denominator.) Velocity measurements involve both systematic and random errors. It is, however, remarkable that the acoustic Doppler current profiler (ADCP) techniques provide almost nonbiased shear measurements (which appear to be limited only by the effects described by *Lien et al.* [1994]), thus substantially reducing the systematic error. As to the random error, it can be significantly reduced by an ensemble averaging.

The Tropical Ocean-Global Atmosphere (TOGA) Coupled Ocean-Atmosphere Response Experiment (COARE) [*Webster and Lukas*, 1992] provided a comprehensive data set on the surface mixed layer of the ocean in the western equatorial Pacific warm pool, including the velocity (ADCP) [*Lukas et al.*, 1995], density [*Huyer et al.*, 1996], and turbulence [*Smyth et al.*, 1996] observations. These data sets are used here to validate the *Ri*-type mixing parameterization explicitly incorporating the physics of the turbulent boundary layer.

The paper is organized as follows. In section 2 the COARE data sets that are used in this paper are described. In section 3
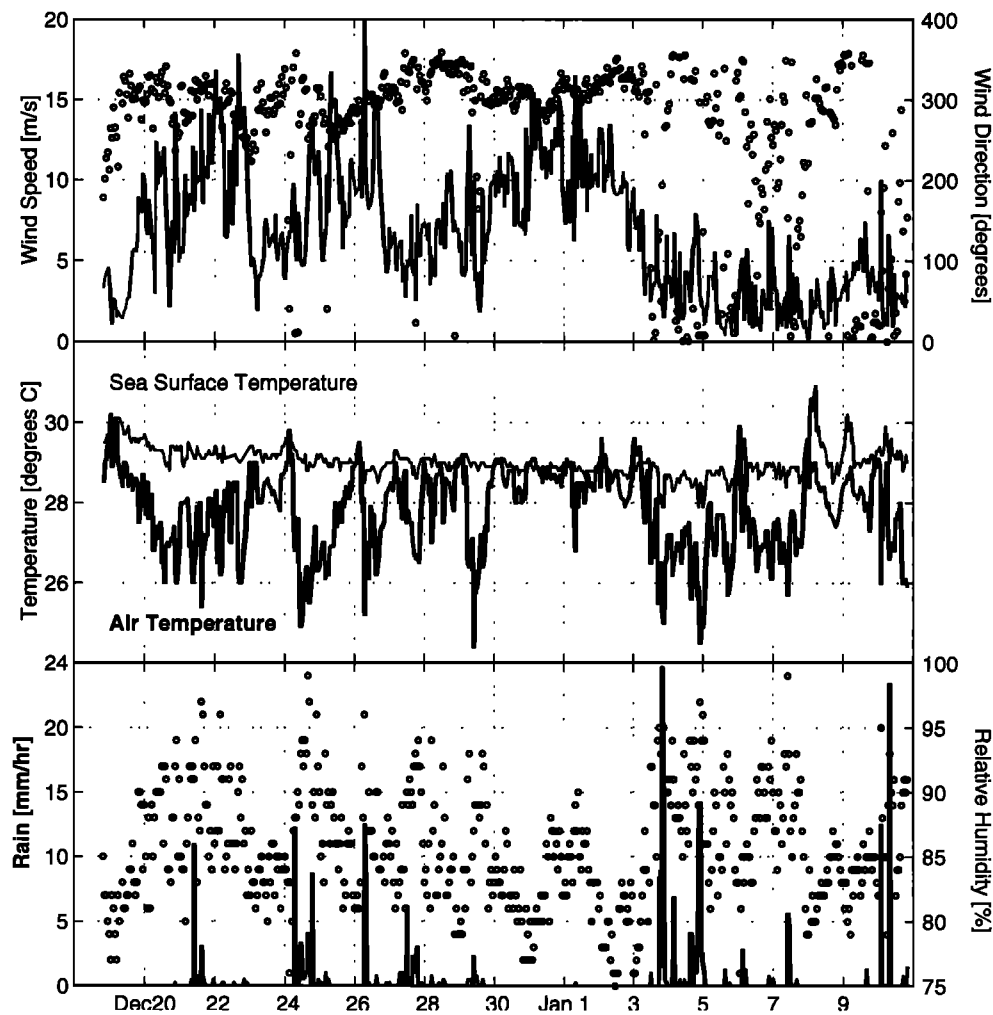

Figure 1. Weather conditions during the R/V *Wecoma* COARE IOP leg 2: (top) the open circles are the wind direction, and the contiguous line is the wind speed; (middle) the upper curve is the water temperature, and the lower curve is the air temperature; and (bottom) open circles are the relative humidity, and the contiguous line is the rain rate.

the theoretical basis for the scaling of planetary boundary layers is summarized on the basis of the previous atmospheric observations. In section 4 the COARE upper ocean velocity and dissipation rate data are scaled as a function of the Richardson number. In section 5 we develop a new parameterization for the vertical mixing coefficient, on the basis of a parameterization scheme using the Ri number and compare it with the TOGA COARE data. In section 6 the new parameterization is tested on several time series starting from a simple extrapolation of the velocity profiles within the mixed layer to a mixed layer model of the diurnal cycle under both low and high wind speed conditions.

2. Data Description

The COARE was conducted in the western equatorial Pacific Ocean to obtain a better understanding of the warm pool system [*Webster and Lukas*, 1992]. This experiment included a 4 month intensive observation period (IOP): from November 1992 through February 1993. Most of the oceanographic and meteorological measurements were taken in the intensive flux array (IFA) centered at 1°45'S, 156°E. As a part of the COARE IOP, the R/V *Wecoma* conducted three survey cruises within the IFA during the following time periods: November 13 to December 2, 1992, December 18 to January 9, 1993, and January 27 to February 15, 1993. Each cruise included the temperature and salinity measurements with a towed vehicle ("Seasoar") undulating in the upper 300 m of ocean, the ADCP velocity measurements within the depth range of 16-300 m, and continuous meteorological observations of wind, air temperature, humidity, etc. [*Lukas et al.*, 1995; *Huyer et al.*, 1997]. The vessel repeated, every 1.5 days, a 130 km by 130 km butterfly pattern centered at 1.8°S, 156.1°E near the Woods Hole Oceanographic Institution (WHOI) surface mooring [*Plueddemann et al.*, 1993]. During the COARE IOP leg 2 cruise the R/V *Moana Wave* sampled the microstructure and turbulence hourly within the depth range from 6 to 250 m and the velocity (ADCP) within the depth range from 14 to 250 m at a position near the WHOI mooring [*Moum and Caldwell*, 1994; *Smyth et al.*, 1996]; this time period, from December 18, 1992 to January 10, 1993, included various forcing conditions (Figure 1).

In this paper (section 6.2.2) we will also use observations in the near-surface layer of the ocean during the COARE Enhanced Monitoring cruise EQ-3. This data set is described by *Soloviev and Lukas* [1997a].

Typical examples of the vertical profiles of the mean current, stratification, stability, and shear parameters in the western Pacific warm pool are shown in Figure 2. These examples are from three west-east R/V *Wecoma* sections during leg 2. Ri is calculated using the "Seasoar" and ADCP gridded data (10 m in depth and ~3 km in horizontal distance) and the formula,

$$Ri = N^2/Sh^2,$$

where $N^2 \approx g\overline{\Delta\rho/\Delta z}$ and $Sh^2 = (\overline{\Delta u/\Delta z})^2 + (\overline{\Delta v/\Delta z})^2$. The averaging is performed on the corresponding depth surfaces along the individual R/V *Wecoma* sections. Note that the terms in the numerator and denominator of the expression for the Richardson number are averaged separately.

The examples shown in Figure 2 comprise conditions of (a) moderate wind speed, (b) westerly wind burst, and (c) calm weather. In the examples given in Figures 2a and 2b the sur-

face mixed layer is clearly seen both in the density and the velocity profiles; the Richardson number within the mixed layer is below its critical value $Ri_{cr}= 1/4$. Under calm weather conditions (Figure 2c) the upper layer of the ocean is restratified, and the Richardson number is greater than its critical value within the analyzed depth range. (Note that from the R/V *Wecoma* data the Richardson number can only be calculated starting from 25 m.) More details about the dynamics of the upper ocean in the western Pacific warm pool during TOGA COARE are given by *Lukas et al.* [1995], *Huyer et al.* [1997], *Moum and Caldwell* [1994], *Wijesekera and Gregg* [1996], and others. See *Godfrey et al.* [1998] for comprehensive references.

3. Boundary Layer Laws

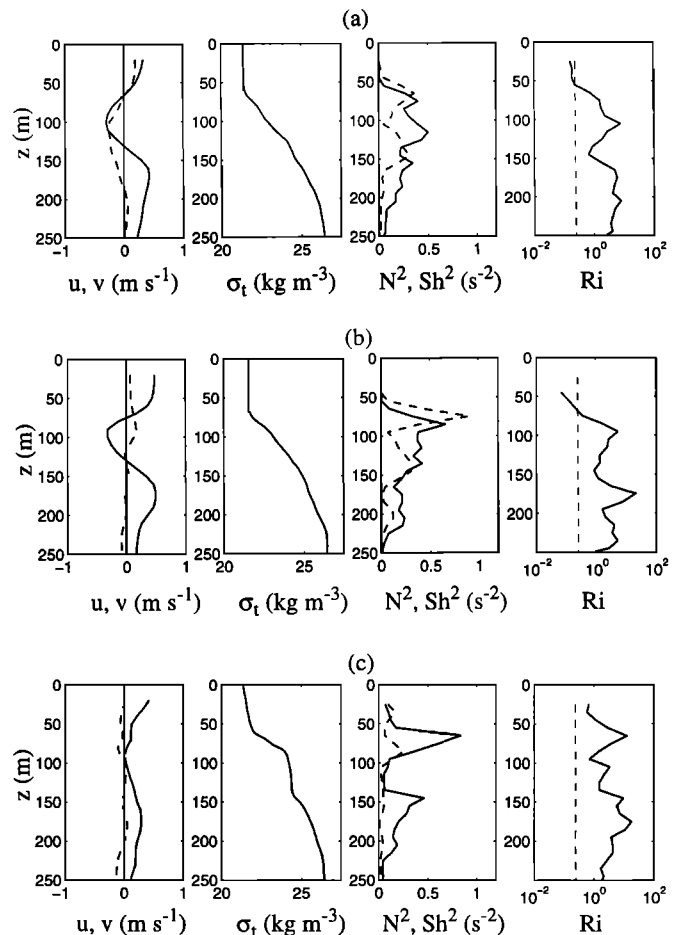The system of equations (A1)-(A6) given in Appendix A suggests that the shear, buoyancy, Coriolis, and pressure gradi-

Figure 2. Examples of averaged vertical profiles from the R/V *Wecoma* COARE IOP leg 2 (east (u) and north (v) velocity, density σ_t, squared Vaisala-Brandt frequency N^2, squared shear Sh^2, and Richardson number Ri): (a) moderate wind speed (December 24, 1992), (b) westerly wind burst (January 1, 1993), and (c) low wind speed (January 10, 1993). The profiles are averaged over the R/V *Wecoma* individual sections (details are in the text). Note that during the westerly wind burst (January 1, 1993) the upper 50 m layer is unstably stratified so the corresponding values of Ri cannot be shown using the logarithmic scale.

Table 1. Order of Magnitude Estimate of Buoyancy (D_B), Rotation (D_E and $D_G \approx L_G$) Length Scales for Different Surface Stress Values[a]

u_*, cm s^{-1}	D_B, m	D_P, m	D_E, m	D_G, m
0.1	0.1[b]	20	50	14
0.5	12.5[b]	100	250	69
1.0	100.0[b]	200	500	137
2.0	800.0	800	1000	274[b]

[a]According to Kraus and Businger [1994], the depth of the mixed layer is $D_B \approx 2L_O$ in the case of no rotation and is $D_E \approx 0.25L_E$ in the case of no stratification. Buoyancy forces apparently dominate over Coriolis forces, when $D_B \ll D_E$.

[b]Minimum values of the length scale.

ent terms may be important in the formation of the vertical structure of the equatorial boundary layer. The process of turbulent mixing can be characterized by its length scale. The estimates of the characteristic length scales for different terms are given in Table 1. Under conditions of low and moderate wind speed prevailing in the warm pool area the buoyancy length scale is typically the minimum one (which means that the buoyancy effects dominate). From length scale considerations it follows that the importance of the horizontal pressure gradient and the horizontal component of Coriolis force increases with wind speed (Table 1). Below we review the buoyancy, rotation, and horizontal pressure gradient effects in more detail.

3.1. Buoyancy Effects

According to the Monin-Oboukhov theory, for the constant stress and heat flux layer the vertical gradients of horizontal velocity u, a scalar property s (e.g., temperature T, salinity S, and density ρ), and the dissipation rate of the turbulent kinetic energy ε may be represented in universal form [Monin and Yaglom, 1971; Businger et al., 1971; Fairall et al., 1980; Kraus and Businger, 1994]:

$$\kappa z u_{*_0}^{-1} \partial u / \partial z = \phi_m(\zeta), \qquad (2a)$$

$$\kappa z s_{*_0}^{-1} \partial s / \partial z = \phi_s(\zeta), \qquad (2b)$$

$$\kappa z \varepsilon / u_{*_0}^3 = \phi_\varepsilon(\zeta), \qquad (2c)$$

where $\zeta = z/L_O$, $s_* = \overline{(w's')}_0/(\kappa u_*)$, $L_O = u_*^3/(\kappa B_0)$, B_0 is the surface buoyancy flux, and u_* is the friction velocity.

A commonly used approximation for the universal functions ϕ_m and ϕ_s, based on atmospheric measurements, is as follows [see Large et al., 1994]:

$$\phi_s \approx \phi_m \approx 1 + \beta\zeta, \quad 0 \le \zeta; \qquad (3a)$$

$$\phi_m \approx (1 - \alpha\zeta)^{-1/4}, \quad \zeta_m \le \zeta < 0; \qquad (3b)$$

$$\phi_m \approx (a_m - c_m\zeta)^{-1/3}, \quad \zeta < \zeta_m, \qquad (3c)$$

$$\phi_s \approx (1 - \alpha\zeta)^{-1/2}, \quad \zeta_s \le \zeta < 0; \qquad (3d)$$

$$\phi_s \approx (a_s - c_s\zeta)^{-1/3}, \quad \zeta < \zeta_s; \qquad (3e)$$

where $\beta = 4$, $\alpha = 16$, $\zeta_m = -0.20$, $\zeta_s = -1.0$, $c_m = 8.38$, $c_s = 98.96$, $a_m = 1.26$, and $a_s = -28.86$. For the dissipation rate, Wyngaard et al. [1971] proposed

$$\phi_\varepsilon(\zeta) = \begin{cases} (1 + 0.5|\zeta|^{2/3})^{3/2}, & \zeta < 0 \\ (1 + 2.5|\zeta|^{2/3})^{3/2}, & \zeta \ge 0 \end{cases}. \qquad (4)$$

The expressions for ϕ_m and ϕ_ρ under stable stratification ($\zeta \ge 0$) may be integrated into dimensionless profiles [Paulson, 1970]:

$$\Delta u / u_* = -(\ln(z/z_0) + \beta\zeta)/\kappa \qquad (5)$$

$$(\rho - \rho_0)/\rho_* = (\ln(z/z_0) + \beta\zeta)/\kappa. \qquad (6)$$

For statistically steady and homogeneous flow the gradient Richardson number can be expressed via dimensionless depth ζ as follows:

$$Ri(\zeta) = \zeta\phi_\rho(\zeta)\phi_m(\zeta)^{-2} \approx \begin{cases} \zeta, & 0 \ge \zeta \ge \zeta_m \\ \zeta/(1 + \beta\zeta), & \zeta > 0 \end{cases}. \qquad (7)$$

For $\zeta > 0$, $Ri(\zeta)$ is monotonically increasing with extremum at $\zeta \to \infty$ ($Ri(\zeta)|_{\zeta \to \infty} = \beta^{-1} = Ri_{cr} \approx 0.25$). The Richardson number within the steady turbulent boundary layer is restricted by its critical value. If the Richardson number exceeds the critical value, this is an indication that this is an area beyond the surface turbulent boundary layer.

The inverse problem can be solved, with ζ being expressed as a function of Ri from (7):

$$\zeta = \begin{cases} Ri, & \zeta_m \le Ri < 0 \\ Ri/(1 - Ri/Ri_{cr}), & 0 \le Ri < Ri_{cr} \end{cases}. \qquad (8)$$

The universal functions ϕ_m, ϕ_s, and ϕ_ε can then be expressed through Ri using (8). (The analytical relationship between Ri and ζ is bulky for $\zeta < \zeta_m \approx -0.20$; therefore it is not shown in (7)-(8).)

The coefficients of turbulent exchange for momentum and a scalar property in the boundary layer are defined as $K_m = u_*^2/\partial u/\partial z$ and $K_s = \overline{(w's')}_0/\partial s/\partial z$, respectively. Using (2a) and (2b), they can be expressed as follows:

$$K_m = \kappa u_* z/\phi_m \qquad (9)$$

$$K_m = \kappa s_* z/\phi_s. \qquad (10)$$

Figure 3 shows different dimensionless characteristics of the turbulent boundary layer plotted versus Ri. The vertical shear and density gradients as well the dissipation rate infinitely increase when Ri approaches its critical value, Ri_{cr} (corresponding to the mixed layer bottom); while the turbulent exchange coefficient vanishes at $Ri \to Ri_{cr}$.

The turbulent boundary layer has the following three asymptotic regimes: (1) logarithmic layer (no stratification effects, i.e., $Ri = 0$), (2) free convection (unstable stratification
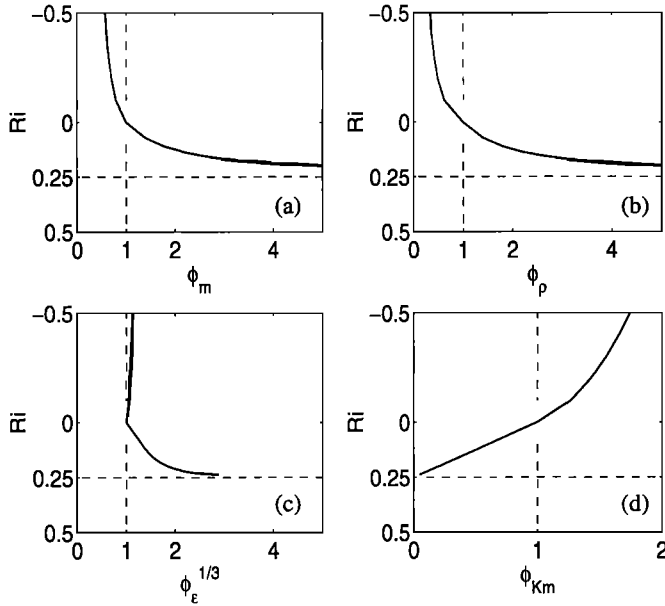
Figure 3. Universal functions for dimensionless (a) shear $\phi_m = (\kappa z/u_*)\partial u/\partial z$, (b) density gradient $\phi_p = (\kappa z/\rho_*)\partial\rho/\partial z$, (c) dissipation rate of the turbulent kinetic energy $\phi_\varepsilon = \varepsilon\kappa z/u_*^3$, and (d) turbulent eddy coefficient $\phi_{K_m} = K_m/(\kappa z u_*)$ expressed via Ri.

and $u_* = 0$, i.e., $Ri = -\infty$), and (3) marginal stability ($Ri = Ri_{cr}$). These asymptotic regimes are discussed below in more detail.

3.1.1. Logarithmic layer. At neutral stratification (i.e., $Ri = 0$) the buoyancy forces are no longer important, and Ri falls out from the set of defining parameters. As a result, function ϕ_m becomes a constant. According to the conventional normalization of ϕ_m, $\phi_m(0) \equiv 1$. The shear and velocity profiles in the logarithmic layer are determined by the following well-known formulas:

$$\partial u/\partial z = u_*/(\kappa z),$$

$$u(z) = (u_*/\kappa)\ln(z/z_0),$$

where z_0 is the roughness length [*Tennekes*, 1973]. The mixing coefficient in the logarithmic layer is as follows:

$$K_0 = \kappa u_* z. \qquad (11)$$

The very near surface part of the oceanic turbulent boundary layer is subject to strong wave influence. The wave dissipation is essentially concentrated within a relatively thin near-surface layer of the ocean, which is equal to about 60% of the significant wave height (A. Soloviev and R. Lukas, Observation of wave-enhanced turbulence in the near-surface layer of the ocean during TOGA COARE, submitted to *Deep-Sea Research*, 2000; hereafter referred to as Soloviev and Lukas, submitted manuscript, 2000). *Csanady* [1984] and *Cheung and Street* [1988] showed that the surface waves influence only the roughness parameter z_0 rather than the logarithmic velocity law.

3.1.2. Free convection. According to *Beljaars* [1994] the mixing coefficients for unstable stratification and zero wind stress can be expressed as follows:

$$K_m = \kappa w_* z, \qquad (12)$$

where $w_* = C(hB_0)^{1/3}$ is the *Priestly* [1959] convective velocity scale, C is the empirical constant close to unity, h is the mixed layer depth, and B_0 is the vertical buoyancy flux. A similar expression can be derived for K_s.

3.1.3. Marginal stability. The situation when Ri is slightly below the critical value is of special interest. In this case the flow is in the so-called regime of marginal stability [*Turner*, 1973]. This is a self-regulated state when the flow adjusts to the existing gross shear and stratification. It is characterized by essentially linear profiles of horizontal velocity and density (note that the linear profiles of density and velocity are the asymptotic limit of relations (5) and (6) at $\zeta \to \infty$). The regime of marginal stability has been observed in the atmospheric boundary layer over the ice in Antarctica, in the nocturnal atmospheric boundary layer, in the outer boundary layer of the gravity current [*Turner*, 1973], during dust storms in the atmosphere [*Barenblatt and Golitsyn*, 1974], and in the equatorial diurnal thermocline [*Kudryavtsev and Soloviev*, 1990].

The self-regulated layer effectively isolates the near-surface turbulent boundary layer from the water below. From (3a), (8), and (9), it follows that for $0 < Ri < Ri_{cr}$,

$$K_m = K_0(1 - Ri/Ri_{cr}), \qquad (13)$$

where $K_0 = \kappa u_* z$ is the coefficient of turbulent mixing in the logarithmic boundary layer. According to (13) the turbulent boundary layer exchange vanishes when $Ri \to Ri_{cr}$. Actually, $K_m|_{Ri = Ri_{cr}} \neq 0$ because there is always some background turbulence below the mixed layer (i.e., at $Ri \geq Ri_{cr}$) caused by the intermittent mixing events. However, $K_m|_{Ri = Ri_{cr}} \ll K_0$.

It should be noted that there are observations of an isolating layer at the bottom of the mixed layer in the western Pacific warm pool. *Lukas and Lindstrom* [1991] called it the barrier layer. The specific mechanism of the barrier layer formation is related to the salinity depression in the upper ocean as a result of enhanced rainfall and horizontal advection. The isolating effect of the barrier layer in the western Pacific warm pool is consistent with the self-regulating state of turbulence near the bottom of the upper ocean boundary layer where the turbulent mixing is greatly reduced by the stratification. However, this analogy is not complete because during certain times the barrier layer may have a significantly overcritical value of the Richardson number [*You*, 1995].

3.2. Rotation Effects

On a rotating sphere with no stratification effects the boundary layer depends on the two components of rotation: $f = 2\Omega\sin\phi$ and $f_y = 2\Omega\cos\phi$, where Ω is the magnitude of the Earth rotation vector and ϕ is the geographical latitude. The Coriolis parameter f results in the Ekman length scale, $L_E = u_*/f$. Because f vanishes at the equator, the classic Ekman layer is too deep to influence strongly the structure of the upper turbulent boundary layer of the equatorial ocean (Table 1). However, the Reynolds stress may interact with the horizontal component of Earth's rotation f_y to exchange turbulent kinetic energy between horizontal and vertical components [*Garwood and Gallacher*, 1985; *Garwood et al.*, 1985], resulting in the length scale $L_G = u_*/(f_y\sin\alpha)$, where α is the wind direction in the meteorological convention (see Appendix A).

3.3. Horizontal Pressure Gradient Effects

In the western Pacific warm pool the surface turbulent boundary layer of the ocean has some unique features because of its proximity to the equator. In Ekman's solution [cf. *Mellor*, 1996] for the drift of water in a rotating homogeneous ocean when acted upon by a steady stress applied to the surface the

(a)

(b)

(c)
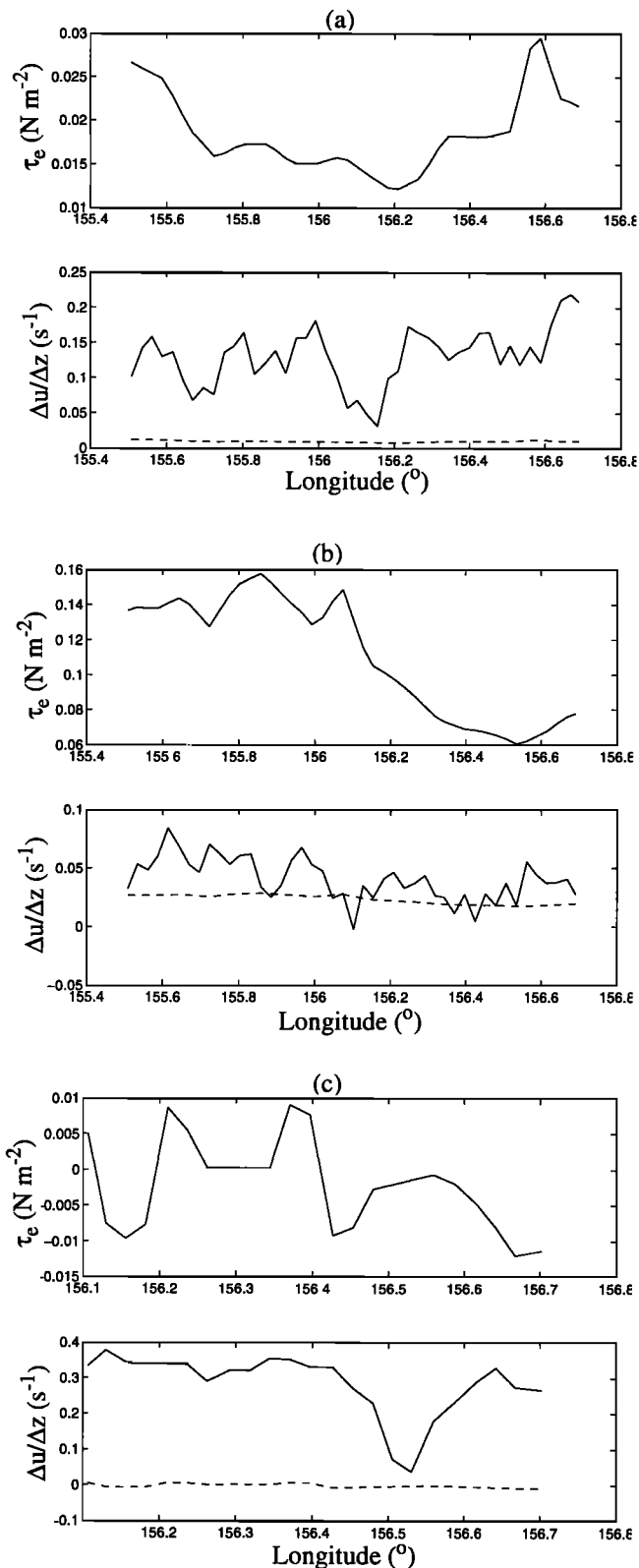
depth of the spiral and the amplitude of the current increase without limit as the vertical component of rotation (or latitude) approaches zero. *Stommel* [1960] was first to show that there is indeed no singularity at the equator. However, to remove the singularity, a zonal pressure gradient is required. At the equator, such a pressure gradient cannot be balanced by the horizontal Coriolis component but must be balanced by friction or inertial forces [*Charney*, 1960]. The wind stress penetrates into the ocean through the surface mixed layer, and the vertical turbulent viscosity provides the principle balance for the zonal pressure gradient driving the undercurrent [*McCreary*, 1981].

It is known from hydraulics engineering that the longitudinal pressure gradient can influence the structure of the turbulent boundary layer [*White*, 1986]. Following *Yaglom* [1979], one can construct the so-called pressure gradient length scale, $L_p = u_*^2/(\rho^{-1} \partial P/\partial x)$. L_p may be derived from the momentum equations under the assumption that the horizontal pressure gradient is approximately balanced by vertical mixing. *Veronis* [1960] related this scale to the depth of the equatorial undercurrent.

4. Boundary Layer Scaling of the Velocity and Dissipation Rate Data from TOGA COARE

Figure 4 shows the observed zonal shear between 20 and 30 m taken during the west-east section of the R/V *Wecoma* under (a) moderate, (b) high, and (c) low wind speed conditions. (These examples correspond to the vertical profiles shown in Figure 2.) The logarithmic layer prediction, which is shown in Figure 4 by dashes, is calculated from the logarithmic layer law (see section 3.1.1) using 30 min wind stress averages. The wind stress is estimated from the R/V *Wecoma* meteorological observations using the COARE 2.5 bulk flux algorithm [*Fairall et al.*, 1996]. The shear calculated from the 20-30 m depth range is close to the logarithmic layer prediction only during extreme conditions of the strong westerly wind burst (Figure 4b). Typically, the logarithmic layer in the warm pool area is shallower than 20 m, and most of the R/V *Wecoma* velocity measurements therefore do not include the logarithmic layer. Because of the substantial observations collected during the 4 month IOP, the number of cases when the logarithmic layer is within the range of the ship's ADCP is, nevertheless, significant. The effects relating to surface wave breaking are essentially localized within the upper few meters of the ocean (see section 3.1.1) and are considered in a separate paper (Soloviev and Lukas, submitted manuscript, 2000).

All observations of shear within the depth range of 20-80 m are plotted in Figure 5 as a function of the Richardson number.

Figure 4. Eastward component of wind stress τ_e and zonal velocity difference between $z_1 = 20$ and $z_2 = 30$ m ($\Delta u/\Delta z$) compared with the logarithmic boundary layer prediction (dashed line) under (a) moderate (December 24, 1992), (b) high (January 1, 1993), and (c) low (January 10, 1993) wind speed conditions. Within the logarithmic boundary layer the velocity difference between two depths z_1 and z_2 is: $\Delta u = (u_{*e}/\kappa)\ln(z_2/z_1)$, where $u_{*e} = \tau_e/(\rho|\tau_e|)^{1/2}$, and eastward component of vertical momentum flux τ_e is calculated from the R/V *Wecoma* meteorological observations using the COARE 2.5 bulk flux algorithm [*Fairall et al.*, 1996].
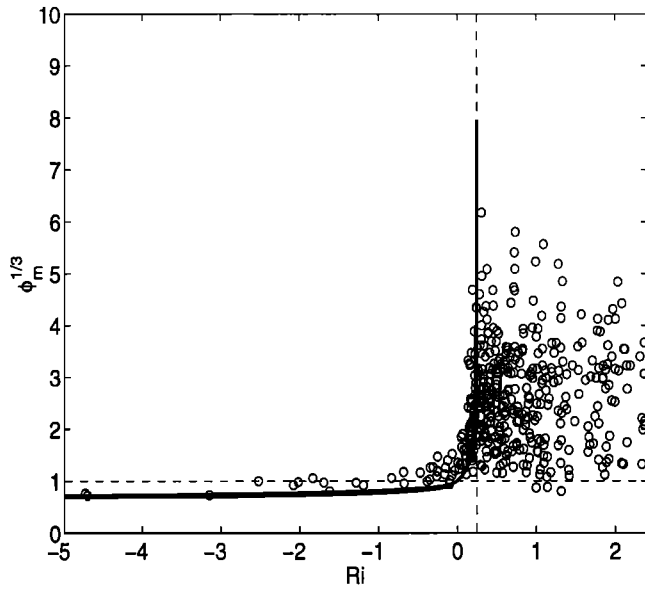
Figure 5. Dimensionless shear $\phi_m = (\kappa z/u_*)\partial u/\partial z$ as a function of Ri. The bold line represents the turbulent boundary layer law from atmospheric measurements. Points are the observations from the depth range of 20-80 m (west-east, north-south, east-north, and south-west sections for all three R/V *Wecoma* IOP legs in the IFA). Measurements taken under light winds ($u_* < 0.3$ cm s^{-1}) are excluded. The vertical dashed line represents the critical value of the Richardson number, $Ri_{cr} = 1/4$; while the horizontal dashed line corresponds to the logarithmic layer dependence.
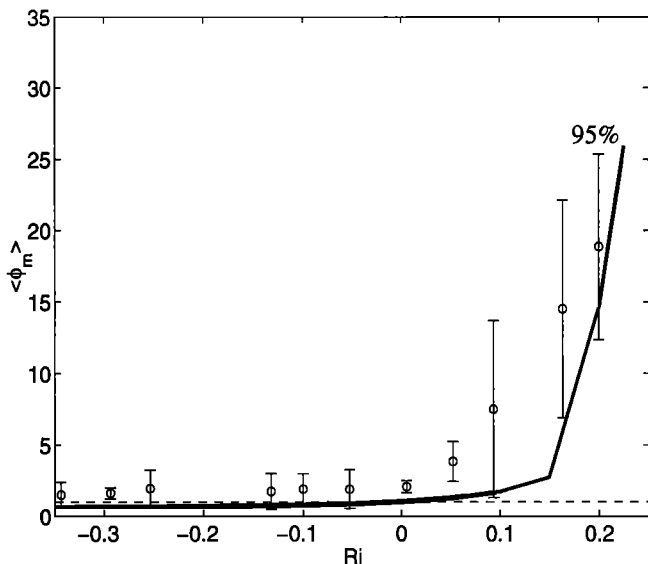

Figure 7. Dimensionless dissipation rate $\phi_\varepsilon = \varepsilon\kappa z/u_*^3$ as a function of Ri. The bold line corresponds to the turbulent boundary layer law. Points are the R/V *Moana Wave* IOP leg 2 data. Dissipation rate of turbulent kinetic energy ε is from *Moum and Caldwell*'s [1994] and *Smyth et al.*'s [1996] turbulence measurements. Friction velocity u_* is calculated from the WHOI mooring meteorology data using the COARE 2.5 bulk flux algorithm [*Fairall et al.*, 1996]. The horizontal dashed line corresponds to logarithmic layer dependence.

Figure 6. Dimensionless shear (from Figure 5) averaged within the mixed layer ($Ri<0.25$). Circles represent the mean for overlapping intervals of $\Delta Ri = 0.1$. The 95% confidence limits are constructed on the basis of Student's distribution [*Rabinovich*, 1995]. The bold line represents the theoretical turbulent boundary layer law averaged over the same Ri intervals. The horizontal dashed line is the logarithmic layer dependence.
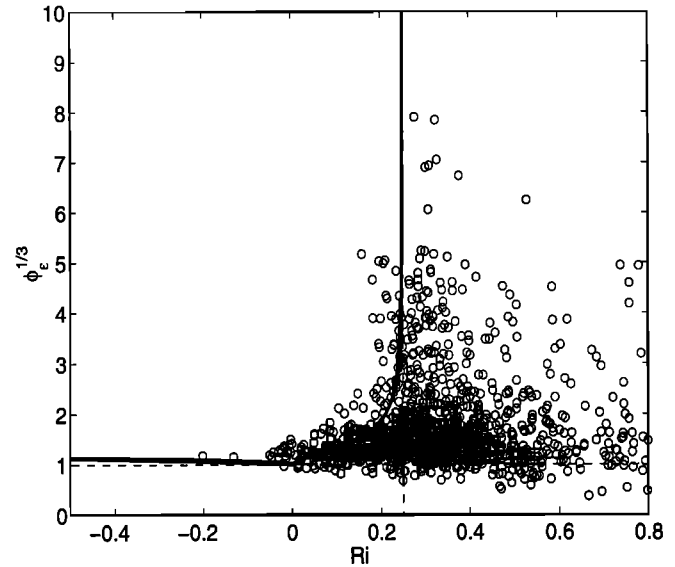
The shear magnitude is normalized on the friction velocity calculated from the R/V *Wecoma* meteorological observations. In Figure 5, there are 17 points within the Richardson number range $-0.1 < Ri < 0.05$ that correspond to the logarithmic layer regime. Most of the ship's ADCP measurements during the R/V *Wecoma* surveys are, however, taken at higher magnitudes of the Richardson number, when the influence of stratification cannot be neglected. The boundary layer (shear) dependence that is shown in Figure 5 with the bold line is similar to that of Figure 3a and accounts for the stratification effects. Within the turbulent boundary layer ($Ri < 0.25$) the boundary layer dependence is consistent with the experimental data; however, the scatter of the individual points is relatively large. At $Ri > 0.25$ the data are more scattered. Note that the universal boundary layer dependences are not defined for $Ri > Ri_{cr}$ (This implies criteria $Ri < Ri_{cr}$ as a definition of the surface mixed layer depth.)

In Figure 6 the shear data for $Ri < Ri_{cr}$ are averaged over the overlapping Richardson number intervals, $\Delta Ri = 0.1$. The averaged shear is shown as a function of the averaged Richardson number. For consistency the theoretical boundary layer dependence is also averaged over the same Ri number intervals on this plot. Within the turbulent boundary layer the averaged dissipation rates are consistent with the theoretical boundary layer dependence, demonstrating the striking effect of increased shear at $Ri \sim Ri_{cr} = 0.25$. Some points, however, deviate from the theoretical dependence by more than the 95% confidence interval.

In Figure 7 dimensionless dissipation rates are plotted as a function of the Richardson number. Measurements made under light winds ($u_* < 0.3$ cm s^{-1}) are excluded. The boundary
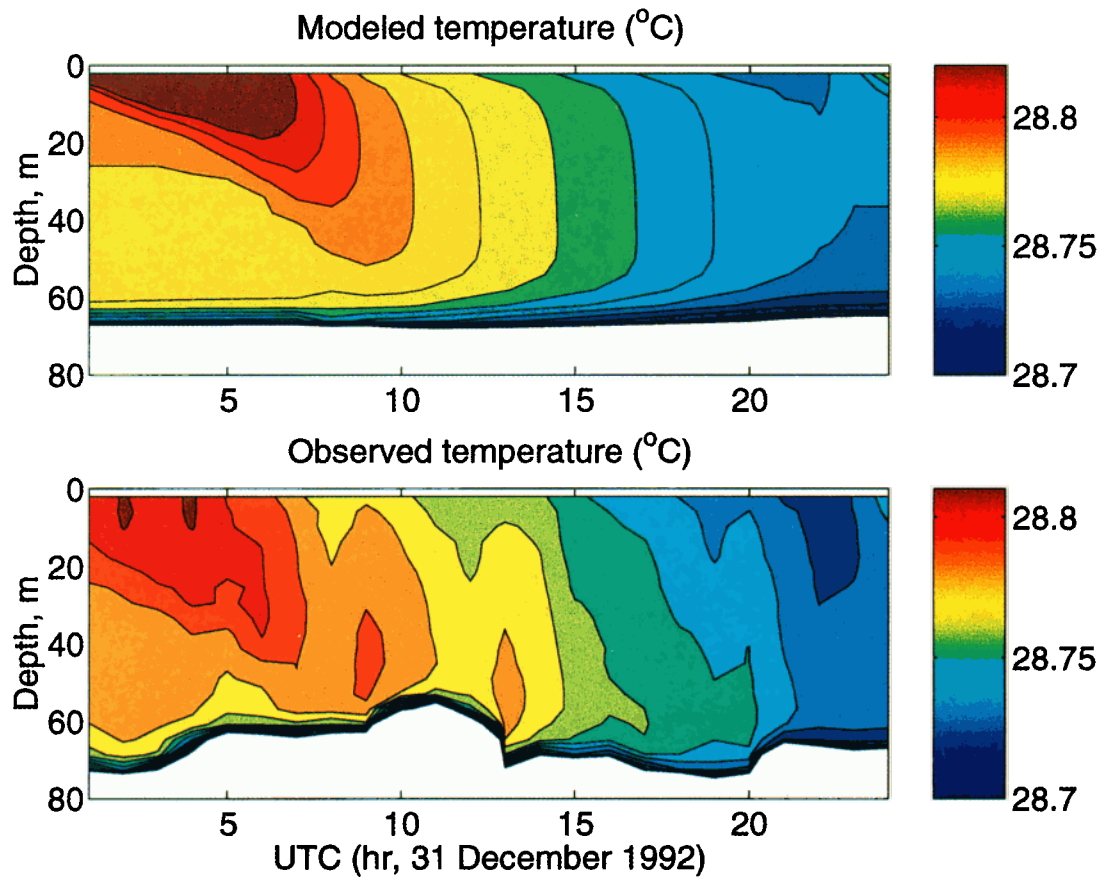
Plate 1. Time-depth section of observed and modeled temperature under conditions of westerly wind burst. The observational data (TOGA COARE) are the same as by *Skyllingstadt et al.* [1999, Figures 3a-3c].

layer dependence for dissipation rate (bold line) is consistent with data within the mixed layer (i.e., at $Ri < Ri_{cr}$). Outside the mixed layer (i.e., at $Ri > Ri_{cr}$), the dimensionless dissipation rate data are almost randomly scattered; this can be explained by the fact that the boundary layer scaling is no longer valid outside the turbulent boundary layer. The rate of turbulence dissipation below the surface mixed layer relates to the statistics of internal wave shear rather than to the surface forcing [*Peters et al.*, 1988]. To some extent, the internal wave breaking events may depend on surface wind stress as well [*Thorpe*, 1975]; this effect is, however, beyond the scope of this paper.

In Figure 8 the averaged dissipation rate data for $Ri < Ri_{cr}$ are presented as in Figure 6. The averaged data are consistent with the boundary layer dependence (three points, however, deviate from the theoretical dependence by more than the 95% confidence interval). The strong increase of the dissipation rate at $Ri \rightarrow 1/4$ is in accordance with the theoretical dependence. Note that the increase of ε at $Ri \rightarrow Ri_{cr}$ is not in contradiction with the decrease of K_m predicted by (13); this is because K_m also depends on the turbulent mixing scale that decreases at $Ri \rightarrow Ri_{cr}$.

5. Parameterization of the Vertical Mixing Coefficient

The upper layer of the western equatorial Pacific warm pool is neither stationary nor horizontally homogeneous [*Huyer et al.*, 1997]. Moreover, the heat and momentum flux within the surface turbulent boundary layer may change with depth.

In this work we propose a mixing parameterization scheme that is based on the gradient Richardson number rather than on the stability parameter ζ. The Ri-type scheme adjusts to the environmental conditions on the relatively short (turbulence) timescale and substantially reduces the effects of nonstationarity.

As to the vertical variation of the wind-induced momentum flux, it is a common problem for scaling the nonstationary oceanic [*Large et al.*, 1994] and atmospheric [*Tennekes*, 1973]
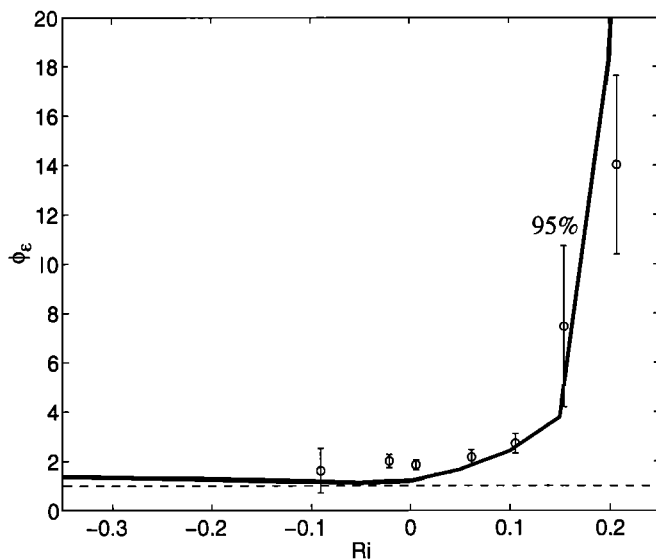

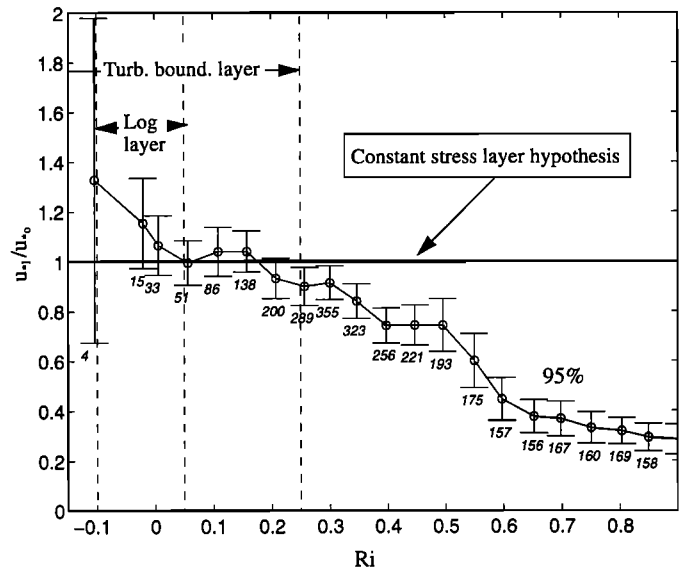**Figure 8.** Dimensionless dissipation rate (from Figure 7) averaged within the mixed layer ($Ri < 0.25$) as in Figure 6.

Figure 9. Test of the constant stress assumption. Friction velocities u_{*l} calculated form the turbulence data [*Moum and Caldwell*, 1994; *Smyth et al.*, 1996] and normalized by surface values u_{*0} are shown as a function of gradient Richardson number. Each circle represents the mean for overlapping intervals of $\Delta Ri = 0.1$; the vertical bars cover the 95% confidence limits, and the numbers below each bar are the number of points averaged. Averaging is done over all profiles (taken every 1 hour) during the R/V *Moana Wave* IOP leg 2. Ri and τ_l are calculated using the data from depth range from 16 to 100 m. Averages over intervals with $Ri < -0.1$ are not shown because there are less than five points falling into these intervals.

boundary layer. To test the constant stress layer hypothesis for the mixed layer in the western Pacific warm pool, we have examined profiles of the local friction velocity, $u_{*l} = (\tau_l/\rho)^{1/2}$, where τ_l is the vertical momentum flux magnitude calculated from Moum and Caldwell's [1994] turbulence measurements. The corresponding surface value u_{*0} has been calculated from the meteorological observations using the COARE 2.5 bulk flux algorithm [*Fairall et al.*, 1996]. Figure 9 shows the mean profile of u_{*l}/u_{*0} as a function of Ri. The number of points within the mixed layer ($Ri < 0.25$) and especially within the logarithmic layer ($-0.1 < Ri < 0.05$) is relatively small. Nevertheless, it is sufficient to provide acceptable confidence intervals within both the mixed layer and the logarithmic layer because of the substantial volume of the data collected during TOGA COARE. According to Figure 9, within the stably stratified mixed layer ($0 < Ri < Ri_{cr}$) the maximum deviation of u_{*l} from its surface value u_{*0} is about 30% and can be approximated as follows:

$$u_{*l} \approx u_{*0}(1 - 0.7 Ri/Ri_{cr}).\qquad(14)$$

A possible approach to account for the vertical momentum flux change with depth (though not following directly from the boundary layer theory but previously employed by several investigators [*McPhee*, 1987; *Large et al.*, 1994]) is to parameterize K_m using the profile of local friction velocity u_{*l} rather than its surface value u_{*0}. This approach will be tested at the end of this section as well.

The mixing parameterization should match to a small but finite turbulence level below the boundary layer. Comprehensive discussions of the eddy momentum exchange coefficient parameterization below the surface turbulent boundary layer are given by *McComas and Muller* [1981], *Peters et al.* [1988], *Gregg et al.* [1993], and *Polzin* [1996]. *Peters et al.* [1988] approximated the momentum eddy coefficient in the upper shear zone, 23-81 m depth, as follows:

$$K_{m_1} = 5.6 \times 10^{-8} Ri^{-8.2} \ \text{m}^2 \ \text{s}^{-1}. \qquad (15)$$

For the higher Ri range, *Peters et al.* [1988] obtained the semiempirical formula

$$K_{m_2} = 5 \times 10^{-4} (1 + 5Ri)^{-1.5} + 2 \times 10^{-5} \ \text{m}^2 \ \text{s}^{-1}. \qquad (16)$$

The final parameterization of the eddy viscosity coefficient K_m by *Peters et al.* [1988] is obtained by adding (15) and (16):

$$K_m = K_{m_1} + K_{m_2}. \qquad (17)$$

The strong power dependence and unboundedness of (15) at $Ri \to 0$ complicates its practical use within the mixed layer.

In this situation we replace (15) with the parameterization of the boundary layer type defined by (9)-(10). From (2a), (2b), (3a), (3b), and (3c), the mixing coefficients for the momentum and a scalar property can be expressed as follows:

$$K_m = \begin{cases} \kappa u_* z (a_m - c_m Ri)^{1/3}, & Ri < Ri_m; \\ \kappa u_* z (1 - \alpha Ri)^{1/4}, & 0 > Ri \ge Ri_m; \\ \kappa u_* z (1 - Ri/Ri_{cr}) + K_{mt}, & 0 \le Ri < Ri_{cr}; \\ K_{mt}, & Ri \ge Ri_{cr}. \end{cases} \qquad (18)$$

$$K_s = \begin{cases} \kappa u_* z (a_s - c_s Ri)^{1/3}, & Ri < Ri_s; \\ \kappa u_* z (1 - \alpha Ri)^{1/4}, & 0 \ge Ri \ge Ri_s; \\ \kappa u_* z (1 - Ri/Ri_{cr}) + K_{st}, & 0 \le Ri < Ri_{cr}; \\ K_{st}, & Ri \ge Ri_{cr}, \end{cases} \qquad (19)$$

where dimensionless constants $Ri_m = -0.20$, $Ri_s = -1.0$, $Ri_{cr} = 0.25$, $\alpha = 16$, $a_m = 1.26$, $a_s = -28.86$, $c_m = 8.38$, and $c_s = 98.96$ are taken from the atmospheric measurements (see section 3.1).

The first two lines in (18) and (19) are the boundary layer parameterization for the unstable stratified mixed layer; the third line is the boundary layer parameterization for the stable stratified mixed layer (which is similar to (13)). K_{mt} is the parameterization of the mixing coefficient for the thermocline, which is primarily intended for $Ri \ge Ri_{cr}$, although is relevant for Ri slightly below Ri_{cr}. We will assume here that $K_{mt} = K_{m_2}$, where K_{m_2} is given by (16). To provide a smooth transition from the mixed layer to the thermocline, the small K_{mt} and K_{st} terms are added to the third lines of (18) and (19) (corresponding to $0 \le Ri < Ri_{cr}$) as well.

To take into account the free convection above a stratified layer, u_* in (18) and (19) can be replaced by $(u_*^2 + w_*^2)^{1/2}$, where w_* is the *Priestly* [1959] convective velocity scale (see section 3.1.2).
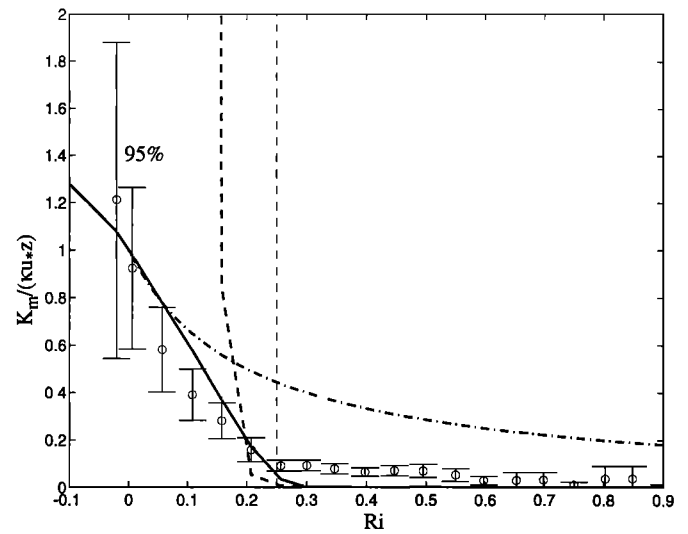

Figure 10. The vertical eddy coefficient for momentum K_m (normalized by logarithmic layer eddy coefficient $\kappa u_* z$) as a function of Ri. Open circles are COARE data from the R/V *Moana Wave* IOP leg 2 [*Moum and Caldwell*, 1994; *Smyth et al.*, 1996]. Each circle represents the mean over Ri intervals as in Figure 6. The solid bold line is parameterization (18). The vertical dashed line corresponds to $Ri = Ri_{cr} = 0.25$. The bold dashed line is the parameterization of *Peters et al.* [1988] calculated for the heat and momentum flux conditions during the R/V *Moana Wave* IOP leg 2. The dash-dotted line is the parameterization $K_m = \kappa u_* z / (1 + 5Ri)$ [*Monin and Yaglom*, 1971].

Figure 10 shows the parameterization (18) in comparison with the momentum mixing coefficient that is derived from the R/V *Moana Wave* COARE IOP leg 2 turbulence data of *Moum and Caldwell* [1994] and *Smyth et al.* [1996]. The vertical momentum mixing coefficient is calculated using the "dissipation method" [*Peters et al.*, 1988]:

$$K_m \approx \bar{\varepsilon} / [(\Delta \bar{u}/\Delta z)^2 + (\Delta \bar{v}/\Delta z)^2],$$

where $\Delta z = 4$ m. The averaged Richardson number is calculated from the formula,

$$Ri \approx g(\Delta \bar{\rho}/\Delta z) / [(\Delta \bar{u}/\Delta z)^2 + (\Delta \bar{v}/\Delta z)^2].$$

The hourly 4 m gridded vertical profiles of the dissipation rate and velocity were averaged at each depth for 12 hours (with a 6 hour overlap). The original data set contained 550 hourly sampled vertical profiles of dissipation rate and velocity. After the averaging it turned out that very few points with the magnitude of the velocity difference, $(\overline{\Delta u^2} + \overline{\Delta v^2})^{1/2} \le 1.2 \times 10^{-3}$ m s^{-1}, produced an enormous scatter in the calculated vertical eddy coefficient and Richardson number compared with the rest of points. These low-shear points (0.99% from the whole data set) are removed from the data set. Finally, the experimental points are averaged over the overlapping Richardson number intervals, $\Delta Ri = 0.1$; confidence intervals are calculated using Student's probability distribution. The average at $Ri = -0.12$ is calculated on four points only; it is not shown here (or in Figure 11) because the confidence interval is quite large.
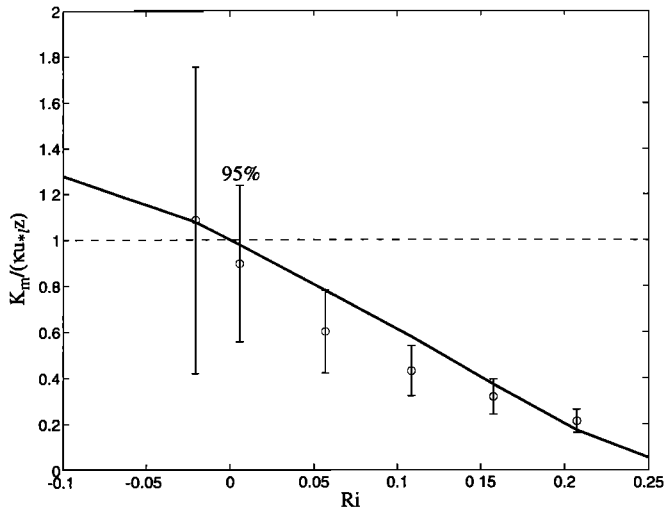
Figure 11. Mixing coefficient K_m normalized by local value of friction velocity u_{*l} (both calculated from COARE turbulence measurements). The solid bold line is parameterization (18); while the horizontal dashed line represents the logarithmic layer.

Two other mixing parameterizations are also shown in Figure 10. The parameterization of *Peters et al.* [1988] is based on the data taken from below the mixed layer, and its comparison with the mixed layer dependence might not be suitable. The parameterization taken from *Monin and Yaglom* [1971] has the correct neutral (logarithmic) layer asymptote, but it is not valid for the unstable stratification and apparently overestimates the mixing coefficient at $Ri > 0.05$.

The important feature of parameterizations (18) and (19) is that they have correct boundary layer asymptotes for stable, unstable, and neutral stratification. As a result, parameterizations (18) and (19) are capable of resolving such details of active mixed layer as the shear and the stratification. The shear and the stratification within the mixing layer are relatively small but dynamically important factors; they are associated with the vertical transfer of buoyancy and momentum.

Figure 11 shows the mixing coefficient K_m scaled with the local friction velocity rather than its surface value. In this case, parameterization (18) is in better agreement with the data; however, the difference is relatively small.

The scaling used in this paper is consistent with the idea that the shear within the mixed layer is proportional to the friction velocity u_* [*Stommel*, 1960; *McPhaden et al.*, 1988]. For the vertical eddy viscosity, *Ekman* [1905, cf. *Santiago-Mandujano and Firing*, 1990] proposed a parameterization $K_m \sim u_*^2$, which is not consistent with the logarithmic layer asymptote observed for neutral stratification conditions in the mixed layer. The analysis of Santiago-Mandujano and Firing [1990] shows that Ekman's $K_m \sim u_*^2$ appears as a result of assuming that the mixed layer depth is proportional to the Ekman scale, $L_E = u_*/f$. This assumption ignores any dependence of K_m on depth z.

The boundary layer parameterization proposed here results in $K_m \sim u_*$, which is consistent with the logarithmic layer asymptote $K_m = \kappa u_* z$. The parameterization of *Large et al.* [1994] based on the boundary layer scaling also infers that $K_m \sim u_*$.

An important feature of turbulence, which has to be taken into account in mixing parameterization schemes, is that it is a fundamentally "nonlocal" process [*Deardorff*, 1972; *Stull and Kraus*, 1987; *Large et al.*, 1994]. This is because the turbulent transport is performed via a cascade of eddies. The nonlocal behavior of turbulence is associated with the presence of spatially coherent organized motions. There are numerous reports about observation of coherent structures in the surface layer of the ocean, including Kelvin-Helmholtz billows [*Thorpe*, 1969], Langmuir cells [*Weller and Price*, 1988; *Walk and Lueck*, 1999], convective plumes and ramp-like structures [*Thorpe*, 1988; *Soloviev*, 1990], and sharp frontal interfaces [*Soloviev and Lukas*, 1997b].

Diffusive models, which are based on the parameterization of turbulent transports by eddy coefficients, are essential local. The large eddy simulation (LES) [*Skyllingstadt et al.*, 1999] and "transilient" [*Stull and Kraus*, 1987] models involve nonlocal features. The nonlocal properties of the turbulence in the mixed layer can be accounted for by including (18)-(19) into the LES or transilient models as the subgrid parameterization. This question is, however, beyond the scope of this paper.

6. Tests of the Boundary Layer Parameterization Using the TOGA COARE Data

6.1. Extrapolation of Velocity Profiles Within Mixed Layer

Within the near-surface mixed layer the boundary layer scaling allows us to extrapolate the velocity profiles up to the ocean surface. However, this is possible only if the reference current meter is within the mixed layer so that $Ri < Ri_{cr}$. Actually, the dependence of the shear on the Richardson number is very steep near $Ri \approx Ri_{cr}$, and the error of the extrapolation increases as Ri_{cr} is approached. In order to limit errors it is reasonable to make the extrapolation only if the current meter is at a depth where $Ri \leq 0.5Ri_{cr}$.

Such an attempt is shown in Figure 12. The WHOI current meter at 19.3 m was used to extrapolate the velocity field to 7.4 m. When both 19.3 and 7.4 m depths are within the turbulent boundary layer the velocity difference is relatively small and is of the order of several cm s^{-1}. The extrapolation is done for the cases when the 12 hour average of the Richardson number is $\leq 0.5Ri_{cr}$. The Richardson number was calculated using the corresponding shear and density profiles measured from the R/V *Moana Wave* located near the WHOI buoy. Comparison of the extrapolated values with the data from the 7.4 m current meter shows the error of extrapolation within approximately 3 cm s^{-1}. For the R/V *Wecoma* data this extrapolation has, of course, limited application since the ADCP minimal depth level is within the turbulent boundary layer only for relatively high wind speed conditions. The total number of cases when $Ri \leq 0.5Ri_{cr}$ is equal to about 15% for the R/V *Moana Wave* IOP leg 2. For comparison, the extrapolation of the velocity profile in the upper 20 m but for the whole R/V *Wecoma* COARE IOP leg 2 using the Price et al. [1986] model shows approximately the same error of extrapolation (P. Hacker and A. Plueddemann, private communication, 1997).

6.2. One-dimensional Model

6.2.1. Equations. To test the boundary layer parameterization derived in section 5, we employ a simple one-dimensional
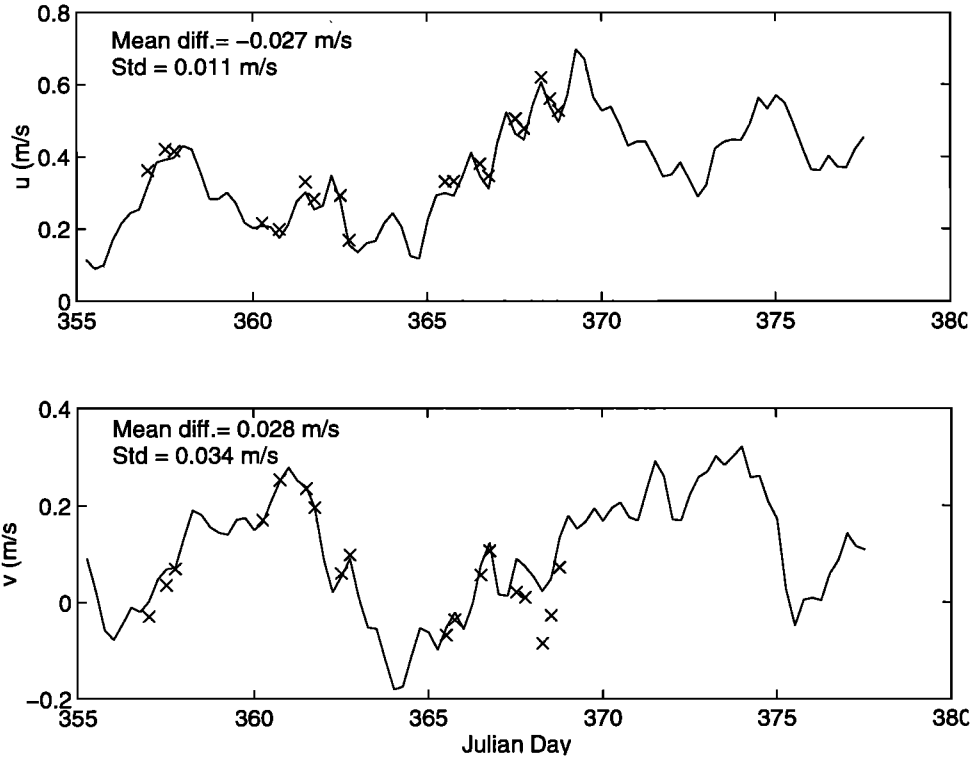
Figure 12. Comparison of the WHOI east (u) and north (v) velocity components at 7.4 m (continuous lines) with corresponding values extrapolated from 19.3 m (crosses) using boundary layer scaling.

(1-D) model. The equations for the heat, salinity, and momentum balance are

$$c_p \rho \partial T / \partial t = -\partial Q / \partial z - \partial Q_R / \partial z,$$ (20)

$$\rho \partial S / \partial t = -\partial F / \partial z,$$ (21)

$$\rho \partial u / \partial t = -\partial \tau_x / \partial z + fv,$$ (22)

$$\rho \partial v / \partial t = -\partial \tau_y / \partial z - fu,$$ (23)

where $Q = -c_p \rho K_t(Ri) \partial T / \partial z$, $F = -\rho K_{sal}(Ri) \partial S / \partial z$, $\tau_x = -\rho K_m(Ri) \partial u / \partial z$; and $\tau_y = -\rho K_m(Ri) \partial v / \partial z$; K_m and K_t are determined from parameterizations (18)-(19) correspondingly, where $K_{sal} = K_t$. The absorption of penetrating solar radiation with depth (Q_R) is parameterized by a nine-exponential dependence in accordance with *Soloviev and Schluessel* [1996]. To calculate the albedo for the short-wave radiation forcing, we used the Fortran code written by Peter A. Coppin (CSIRO Centre for Environmental Mechanics, Australia), employing the Payne [1972] model.

To test our boundary layer parameterization within the 1-D model, we selected two examples from the TOGA COARE data: (1) the diurnal cycle under low wind speed conditions (May 4, 1994); and (2) the diurnal cycle under conditions of westerly wind burst (December 31, 1992). The model ((20)-(23)) is forced by the wind stress and sensible and latent heat fluxes calculated using the COARE 2.5 bulk flux algorithm [*Fairall et al.*, 1996]. The net long-wave radiation flux is calculated using parameterization of *Simpson and Paulson* [1979].

6.2.2. Diurnal cycle under low wind speed conditions.
For simulation of the diurnal cycle on May 4, 1994 (Figure 13) we used 20 evenly spaced grid points within the top 10 m of the ocean. The vertical resolution and the time step were 0.5 m and 0.4 s, respectively. The vertical profiles of the temperature and salinity were initialized to be a constant in the upper 20 m of the ocean, while the velocity profile was initialized by a 0.0004 s⁻¹ shear to avoid infinite values of the Richardson number at the first step of the simulation. The mixing parameterization includes the wave-breaking term proposed by *Soloviev and Lukas* (submitted manuscript, 2000) on the basis of the *Craig and Banner* [1994] model.

According to Figure 13 the model reproduces the main features of the diurnal cycle observed on May 4, 1994. Including the horizontal component of the Coriolis acceleration in the parameterization of the mixing coefficient, using formula (A13), does not result in any appreciable change of the model output. This is similar to the conclusion of *Wang et al.* [1996] based on the LES of the diurnal cycle in the equatorial ocean.

6.2.3. Diurnal cycle under high wind speed conditions.
For simulation of the diurnal cycle on December 31, 1992 (Plate 1), we used 50 evenly spaced grid points within the top 100 m of the ocean. The vertical resolution and the time step were 2 m and 1 s, respectively. The vertical profiles of the temperature, salinity, and zonal and meridional velocity are taken from the measurements made on 31 December 31, 1992, at 0000 UTC.

Within the mixed layer the observed diurnal cycle of temperature is well reproduced by the model (Plate 1). The biggest difference is at the bottom of the mixed layer, which is influenced by baroclinic waves, so we do not expect perfect agreement in this area.
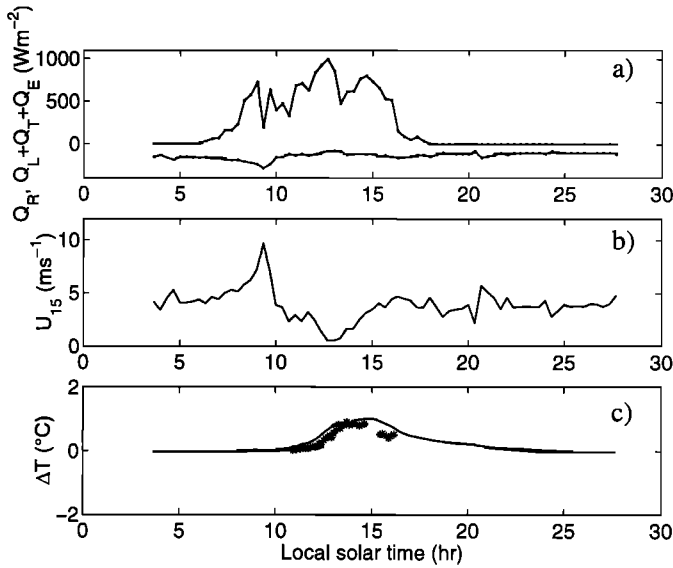
Figure 13. Evolution of the temperature difference in the near-surface layer of the ocean under low wind speed conditions: (a) solar insolation (Q_R) and surface cooling heat fluxes ($Q_0 = Q_L + Q_T + Q_E$), (b) wind speed at 15 m height; (c) temperature difference $\Delta T = T_0 - T_8$ in the near-surface layer of the ocean as measured by free-rising profiler (asterisks) and simulated by the 1-D model employing parameterizations (18)-(19) (contiguous line). Here T_0 and T_8 are the temperatures averaged over depth range 0-0.25 and 8-8.25 m, respectively. The field data are the same as by *Soloviev and Lukas* [1997a, Figure 8].

The same example as in Plate 1 had been modeled by a LES model [*Skyllingstadt et al.*, 1999, Figure 3]. For this case our simple 1-D model has approximately the same performance as the LES model. Including the horizontal component of the Coriolis acceleration into the parameterization of the mixing coefficient, using formula (A13), results only in a minor change of the model output.

7. Conclusions

1. The boundary layer scaling of the oceanic surface mixed layer developed in this work is consistent with such features as the barrier layer, strong shear, and increased dissipation rate between the base of the shallow mixed layer and the top of the relatively deep thermocline, the features often observed in the warm pool area [*Lukas and Lindstrom*, 1991; *Lukas et al.*, 1995; *Moum and Caldwell*, 1994]. The corresponding mixing parameterizations for momentum (18) and a scalar property (19) are valid for both stable and unstable stratification in the upper ocean and are compatible with the nonstationary and horizontally heterogeneous atmospheric forcing. An important feature of parameterizations (18)-(19) is that they have the true turbulent boundary layer asymptotes, which allows us to resolve the details of the active mixing layer, the shear and stratification near its surface and bottom.

2. Parameterizations (18)-(19) have been successfully tested within the framework of a 1-D model on two examples obtained during the TOGA COARE. This parameterization scheme, however, needs more comparison tests to understand its performance relative to the other schemes [e.g., *Price et al.*,

1986; *Large et al.*, 1994; *Mellor and Yamada*, 1982]. To account for the nonlocal turbulent transport, the new parameterization may be implemented into transilient- or LES-type models.

Appendix A: Components of the Coriolis Acceleration Near the Equator

According to *Mellor* [1996] the components of the momentum equation on a rotating sphere in the Boussinesq approximation are the following:

$$\rho_0\left(\frac{Du}{Dt} - fv + f_y w\right) = -\frac{\partial p}{\partial x} + \frac{\partial \tau_{xx}}{\partial x} + \frac{\partial \tau_{yx}}{\partial y} + \frac{\partial \tau_{zx}}{\partial z}, \quad (A1)$$

$$\rho_0\left(\frac{Dv}{Dt} + fu\right) = -\frac{\partial p}{\partial y} + \frac{\partial \tau_{xy}}{\partial x} + \frac{\partial \tau_{yy}}{\partial y} + \frac{\partial \tau_{zy}}{\partial z}, \quad (A2)$$

$$\rho_0\left(\frac{Dw}{Dt} - f_y u\right) = -\rho g + \frac{\partial p}{\partial z} + \frac{\partial \tau_{xz}}{\partial x} + \frac{\partial \tau_{yz}}{\partial y} + \frac{\partial \tau_{zz}}{\partial z}, \quad (A3)$$

where ρ_0 is the density that in many oceanic applications may be taken as a constant;

$$\frac{DF}{Dt} = u\frac{\partial F}{\partial x} + v\frac{\partial F}{\partial y} + w\frac{\partial F}{\partial z} + \frac{\partial F}{\partial t},$$

where F is u, v, or w; the rectangular coordinate system has its origin at the sea surface, with x directed eastward, y directed northward, z directed upward, and u, v, and w represent the corresponding ensemble mean velocity components; t is the time; $f = 2\Omega\sin\phi$ and $f_y = 2\Omega\cos\phi$, where Ω is the magnitude of the Earth's rotation vector and ϕ is the latitude; p is pressure; τ denotes different components of the turbulent stress; g is the acceleration of gravity; and ρ is the water density at the gravity term. According to the order of magnitude estimate [*Mellor*, 1996] the term containing the y component of Coriolis acceleration in (A1), $f_y w$, is much less than other terms. At the equator the z component of Coriolis acceleration (f) is equal to zero and the corresponding terms in (A1) and (A2) vanish. The y Coriolis acceleration is nonzero at the equator; however, the y Coriolis terms in the x and z component of the momentum equation, (A1) and (A3), are still much smaller than the other terms and are usually neglected in the models of equatorial dynamics [see, e.g., *Moore and Philander*, 1977].

The individual turbulent kinetic energy budgets are given in the following form [*Garwood*, 1977]:

$$\frac{1}{2}\frac{\partial \overline{u'^2}}{\partial t} = -\overline{u'w'}\frac{\partial u}{\partial z} - \frac{\partial}{\partial z}\left(\frac{\overline{w'u'^2}}{2}\right) + \frac{\overline{p'}}{\rho_0}\frac{\partial u'}{\partial x} + f\overline{u'v'} - f_y\overline{u'w'} - \frac{\varepsilon}{3}, \quad (A4)$$

$$\frac{1}{2}\frac{\partial \overline{v'^2}}{\partial t} = -\overline{v'w'}\frac{\partial v}{\partial z} - \frac{\partial}{\partial z}\left(\frac{\overline{w'v'^2}}{2}\right) + \frac{\overline{p'}}{\rho_0}\frac{\partial}{\partial y}v' - f\overline{u'v'} - \frac{\varepsilon}{3}, \quad (A5)$$

$$\frac{1}{2}\frac{\partial \overline{w'^2}}{\partial t} = \overline{b'w'} - \frac{\partial}{\partial z}\left(\frac{\overline{w'^3}}{2} + \frac{\overline{w'p'}}{\rho_0}\right) + \frac{\overline{p'}}{\rho_0}\frac{\partial}{\partial z}w' + f_y\overline{u'w'} - \frac{\varepsilon}{3}, \quad (A6)$$

where ε is the viscous dissipation and prime denotes the fluctuating components. *Garwood and Gallacher* [1985] studied

the usually neglected y Coriolis term in the turbulent kinetic energy budget of the surface turbulent boundary layer $(f_y u'w')$. In this term the Reynolds stress interacts with the northward component of planetary rotation to exchange turbulent kinetic energy between horizontal and vertical components.

For the no-entrainment condition and a positive downward buoyancy flux B_0, *Garwood and Gallacher* [1985] suggested the following expression for the mixed layer depth:

$$h = C_1 L_O/(1 + C_2 \Phi), \quad (A7)$$

where C_1 and C_2 are the dimensionless constants ($C_1 = 1$ and $C_2 = 12/7$) and $\Phi = \Omega_y \tau_x/(\rho B_0)$. From (A7) it follows that to account for the y component of the Coriolis acceleration on the equator, the Oboukhov length scale can be modified in the following way:

$$L_O' = C_1 L_O/(1 + C_2 \Phi). \quad (A8)$$

where $L_O = u_*^3/(\kappa B_O)$. Taking into account that $\tau_x = -u_*^2 \sin\alpha$, where τ is the wind stress magnitude, and α is the wind direction in the meteorological convention, formula (A.8) can be rewritten in the following way:

$$L_O' = C_1 L_O/(1 - C_2 \kappa L_O/L_G). \quad (A9)$$

where $L_G = u_*/(f_y \sin\alpha)$.

Resolving (A9) with respect to L_O, we obtain a relationship

$$L_O = L_O'/(C_1 + C_2(\kappa L)/L_G), \quad (A10)$$

which is useful to express the Richardson number,

$$Ri = g(\partial\rho/\partial z)/(\partial u/\partial z)^2 = zL_O^{-1}\phi_\rho(\zeta')\phi_m(\zeta')^{-2}, (A11)$$

via the stability parameter $\zeta' = z/L_O'$. Combining (A10), (A11), and (3a), we obtain the following interconnection between Ri and ζ: $Ri = \zeta'[1 + C_2(\kappa z/L_G)\zeta'^{-1}](1 + \beta\zeta')^{-1}$ or, in the inverted form,

$$\zeta' = (Ri - C_2\kappa z/L_G)(1 - Ri/Ri_{cr})^{-1}. \quad (A12)$$

Using (A12), the effect of the y component of the Coriolis acceleration on the turbulent mixing coefficient can be expressed via the gradient Richardson number,

$$K_m = u_{*_0}^2/\partial u/\partial z = u_{*_0}^2/\phi_m(\zeta') \quad (A13)$$
$$= u_{*_0}^2/(1 + \beta\zeta') = \gamma\kappa u_{*_0}z(1 - Ri/Ri_{cr}),$$

where $\gamma = (1 - C_2 Ri_{cr}^{-1}\kappa z/L_G)^{-1}$. Comparison of (A13) to (13) shows that the factor γ accounts for the y component Coriolis acceleration effect.

References

Barenblatt, G.I., and G.S. Golitsyn, Local structure of mature dust storms, *J. Atmos. Sci., 31,* 1917-1933, 1974.

Beljaars, A.C.M., The parameterization of surface fluxes in large-scale models under free convection, *Q. J. R. Meteorol. Soc., 121,* 255-270, 1994.

Businger, J.A., J.C. Wyngaard, Y. Izumi, and E.F. Bradley, Flux-profile relationships in the atmospheric surface layer, *J. Atmos. Sci., 28,* 181-189, 1971.

Charney, J.G., Non-linear theory of a wind-driven homogeneous layer near the equator, *Deep Sea Res., 6,* 303-310, 1960.

Cheung, T.K., and R.L. Street, The turbulent layer in the water at an air-water interface, *J. Fluid Mech., 194,* 133-151, 1988.

Craig, P.D., and M.L. Banner, Modeling wave-enhanced turbulence in the ocean surface layer, *J. Phys. Oceanogr., 24,* 2546-2559, 1994.

Csanady, G.T., The free surface turbulent shear layer, *J. Phys. Oceanogr., 14,* 402-411, 1984.

Deardorff, J.W., Numerical investigations of neutral and unstable planetary boundary layers, *J. Atmos. Sci., 29,* 91-115, 1972.

Ekman, V.W., On the influence of the earth's rotation on ocean currents, *Arc. Mat., Astron, Fys., 2,* 1-53.

Fairall, C.W., R. Markson, G.E. Schacher, and K.L. Davidson, An aircraft study of turbulence dissipation rate and temperature structure function in the unstable marine atmospheric boundary layer, *Boundary Layer Meteorol., 19,* 453-469, 1980.

Fairall, C., E.F. Bradley, J.B. Edson, and G.S. Young, The TOGA COARE Bulk Flux Algorithm, *J. Geophys. Res., 101,* 3747-3764, 1996.

Garwood, R.W., Jr., An oceanic mixed layer model capable of simulating cyclic states, *J. Phys. Oceangr., 7,* 455-468, 1977.

Garwood, R.W., Jr., and P.C. Gallacher, Wind direction and equilibrium mixed layer depth: General theory, *J. Phys. Oceanogr., 15,* 1325-1331, 1985.

Garwood, R.W., Jr., P. Muller, and P.C. Gallacher, Wind direction and equilibrium mixed layer depth in the tropical Pacific ocean, *J. Phys. Oceanogr., 15,* 1332-1338, 1985.

Godfrey, J.S., R.A. Houze Jr., R.H. Johnson, R. Lukas, J.-L. Redelsperger, A. Sumi, and R. Weller, Coupled Ocean-Atmosphere Response Experiment (COARE): An interim report, *J. Geophys. Res., 103,* 14,395-14,450, 1988.

Gregg, M.C., H.E. Seim, and D.B. Percival, Statistics of shear and turbulent dissipation profiles in random internal wave fields, *J. Phys. Oceanogr., 23,* 1777-1979, 1993.

Huyer, A., P.M. Kosro, R. Lukas, and P. Hacker, Upper-ocean thermohaline fields near 2°S, 156°N during TOGA COARE, November 1992 to February 1993, *J. Geophys. Res, 102,* 12,749-12,784, 1997.

Kraus, E.B., and J.A. Businger, *Atmosphere-Ocean Interaction,* Oxford Univ. Press, New York, 1994.

Kudryavtsev, V.N., and A.V. Soloviev, Slippery near-surface layer of the ocean arising due to daytime solar heating, *J. Phys. Oceanogr., 20,* 617-628, 1990.

Lagerloef, G.S.E., R. Lukas, R.A. Weller, and S.P. Anderson, Pacific warm pool sea surface temperature regulation as indicated by a stochastic model and TOGA COARE measurements, *J. Clim., 11,* 2297-2309, 1998.

Large, W.G., J.C. McWilliams, and S.C. Doney, Oceanic vertical mixing: A review and a model with a nonlocal boundary layer parameterization, *Rev. Geophys., 32,* 363-403, 1994.

Lien, R.-C., M.J. McPhaden, and D. Hebert, Intercomparison of ADCP measurements at 0°, 140°W. *J. Atmos. Oceanic Technol., 11,* 1334-1349, 1994.

Lukas, R., and E. Lindstrom, The mixed layer of the western equatorial Pacific Ocean, *J. Geophys. Res., 96,* 3343-3357, 1991.

Lukas, R., P. Hacker, M. Mao, E. Firing, A. Huyer, and P.M. Kosro, Upper ocean currents in the intensive flux array during TOGA COARE, in *TOGA 95 Conference Proceedings, WMO/TD 717,* pp. 542-546, World Meteorol. Org., Geneva, 1995.

McComas, C.H., and P. Muller, The dynamic balance of internal waves, *J. Phys. Oceanogr., 11*, 970-986, 1981.

McCreary, J.P., A linear, stratified ocean model of the equatorial undercurrent, *Philos. Trans. R. Soc. London, Ser. A, 298*, 603-635, 1981.

McPhaden, M.J., H.P. Freitag, S.P. Hayes, B.A. Taft, Z. Chen, and K. Wirtki, The response of the equatorial Pacific Ocean to a westerly wind burst in May 1986, *J. Geophys. Res., 93*, 10,589-10,603, 1988.

McPhee, M.G., A time dependent model for turbulent transfer in a stratified oceanic boundary layer, *J. Geophys. Res., 92*, 6977-6986, 1987.

Mellor, G.L., *Introduction to Physical Oceanography*, 260 pp., AIP Press, Woodbury, N.Y., 1996.

Mellor, G.L. and T. Yamada, Development of a turbulence closure model for geophysical fluid problems, *Rev. Geophys., 20*, 851-875, 1982.

Monin, A.S. and A.M. Yaglom, *Statistical Fluid Mechanics*, vol. 1, MIT Press, Cambridge, Mass., 1971.

Moore, D.W., and S.G.H. Philander, Modeling of the tropical ocean circulation, in *The Sea*, vol. 6, *Marine Modeling*, pp. 319-361, Wiley-Interscience, New York: 1977.

Moum, J.N. and D.R. Caldwell, Experiment explores the dynamics of the ocean mixing, *Eos, Trans., AGU, 75*, 489, 494-495, 1994.

Pacanowski, R.C., and S.G.H. Philander, Parameterization of vertical mixing in numerical models of tropical oceans, *J. Phys. Oceanogr., 11*, 1443-1451, 1981.

Paulson, C.A., The mathematical representation of wind speed and temperature profiles in the unstable atmospheric surface layer, *J. Appl. Meteorol., 9*, 857-861, 1970.

Payne, R.E., Albedo of the sea surface, *J. Atmos. Sci., 29*, 959-970, 1972.

Peters, H., M.C. Gregg, and J.M. Toole, On the parameterization of equatorial turbulence, *J. Geophys. Res., 93*, 1199-1218, 1988.

Plueddemann, A.J., R.P. Trsak, W.M.Ostrom, R.A. Weller, B.S. Way, S.P. Anderson, N. Bogue, J. Shillingford, and S. Hill, TOGA COARE mooring deployment check-out, and recovery cruises, *Tech. Rep. WHOI-93-30*, 54 pp., Woods Hole Oceanogr. Inst., Woods Hole, Mass., 1993.

Polzin, K., Statistics of the Richardson number mixing models and finestructure, *J. Phys. Oceanogr., 26*, 1409-1425, 1996.

Price J., R. Weller, and R. Pinkel, Diurnal cycling: Observations and models of the upper ocean response to diurnal heating, cooling and wind mixing, *J. Geophys. Res., 91*, 8411-8427, 1986.

Priestly, C.H.B., *Turbulent Transfer in the Lower Atmosphere*, 130 pp., Univ. of Chicago Press, Chicago, Ill., 1959.

Rabinovich, S.G., *Measurement Errors: Theory and Practice*, 279 pp., AIP Press, Woodbury, N.Y., 1995.

Robinson, A.R., The general thermal circulation in equatorial regions, *Deep Sea Res., 6*, part A, 311-317, 1960.

Santiago-Mandujano, F., and E. Firing, Mixed-layer shear generated by wind stress in the central equatorial Pacific, *J. Phys. Oceanogr., 20*, 1576-1582, 1990.

Simpson, J.J., and C.A. Paulson, Mid-ocean observations of atmospheric radiation, *Q. J. R. Meteorol. Soc., 105*, 487-502, 1979.

Skyllingstadt, E.D., W.D. Smyth, J.N. Moum, and H. Wijesekera, Upper ocean turbulence during a westerly wind burst: A comparison of large-eddy simulation results and microstructure measurements, *J. Phys. Oceanogr., 29*, 5-28, 1999.

Smyth, W.D., D. Hebert, and J.N. Moum, Local ocean response to a multiphase westerly wind burst, 1, Dynamic response, *J. Geophys. Res., 101*, 22,495-22,512, 1996.

Soloviev, A.V., Coherent structure at the ocean surface in convectively unstable conditions. *Nature, 346*, 157-160, 1990.

Soloviev, A., and R. Lukas, Observation of large diurnal warming events in the near-surface layer of the western equatorial Pacific warm pool. *Deep Sea Res., 44*, part A, 1055-1076, 1997a.

Soloviev, A., and R. Lukas, Sharp frontal interfaces in the near-surface layer of the ocean in the western equatorial Pacific warm pool, *J. Phys. Oceanogr., 27*, 999-1017, 1977b.

Soloviev, A.V., and P. Schluessel, Evolution of cool skin and direct air-sea gas transfer coefficient during daytime, *Boundary Layer Meteorol., 77*, 45-68, 1996.

Soloviev, A., R. Lukas, and P. Hacker, An approach to parameterization of the oceanic turbulent boundary layer in the western Pacific warm pool, in *Proceedings of a Conference on the TOGA Coupled Ocean-Atmosphere Experiment COARE, WMO/TD 940*, pp. 367-368, World Meteorol. Org., Geneva, 1999.

Stommel, H., Wind-drift near the equator, *Dee- Sea Res., 6*, part A, 298-302, 1960.

Stull R.B., and E.B. Kraus, The transilient model of the upper ocean, *J. Geophys. Res, 92*, 10,745-10,755, 1987.

Tennekes, H., The logarithmic wind profile, *J. Atmos. Sci., 30*, 558-567, 1973.

Thorpe, S.A., Experiments on the instability of stratified shear flows: immiscible fluids, *J. Fluid Mech., 39*, 25-48, 1969.

Thorpe, S.A., The excitation, dissipation and interaction of internal waves in the deep ocean, *J. Geophys. Res., 80*, 328-338, 1975.

Thorpe, S.A., The dynamics of the boundary layers of the deep ocean. *Sci. Prog. Oxford, 72*, 189-206, 1988.

Turner, J.S., *Buoyancy Effects in Fluids*, Cambridge Univ. Press, New York, 1973.

Veronis, G., An approximate theoretical analysis of the equatorial undercurrent, *Deep Sea Res., 6*, part A, 318-327, 1960.

Walk, F.A.B., and R.G. Lueck, Near-surface heat flux and Langmuir circulation results from measurements with a towed vehicle (abstract), *Eos, Trans., AGU*, 1999 Spring Meet. Suppl., 192, 1999.

Wang, D., W.G. Large, and L.C. McWilliams, Large-eddy simulation of the equatorial ocean boundary layer: Diurnal cycling, eddy viscosity, and horizontal rotation, *J. Geophys. Res., 101*, 3649-3662, 1996.

Webster, P.J., and R. Lukas, TOGA COARE: The Coupled Ocean-Atmosphere Response Experiment, *Bull. Am. Meteorol. Soc., 73*, 1377-1416, 1992.

Weller, R.A., and J.F. Price, Langmuir circulation within the oceanic mixed layer, *Deep Sea Res., 35*, part A, 711-747, 1988.

White, F.M., *Fluid Mechanics*, 732 pp., McGraw-Hill, New York, 1986.

Wijesekera, H.W., and M.C. Gregg, Surface layer response to weak winds, westerly bursts, and rain squalls in the western Pacific warm pool, *J. Geophys. Res., 101*, 977-997, 1996.

Wyngaard, J.C., O.R. Cote, and Y. Izumi, Local free convection similarity, and the budgets of shear stress and heat flux, *J. Atmos. Sci., 28*, 1172-1182, 1971.

Yaglom, A.M., Similarity laws for constant-pressure and pressure-gradient turbulent flows, *Annu. Rev. Fluid Mech., 11*, 505-540, 1979.

You, Y., Salinity variability and its role in the barrier-layer formation during TOGA-COARE, *J. Phys. Oceanogr., 25*, 2778-2807, 1995.

Yu, Z., and P.S. Schopf, Vertical eddy mixing in the tropical upper ocean: Its influence on zonal currents, *J. Phys. Oceanogr., 27*, 1447-1458, 1997.

Zilitinkevich, S.S., A.S. Monin, and D.V. Chalikov, Interaction of the ocean and atmosphere, in *Physics of the Ocean*, vol. 1, edited by V.M. Kamenkovich and A.S. Monin, pp. 208-339, Nauka, Moscow, 1978.

P. Hacker and R. Lukas, School of Ocean and Earth Science and Technology, University of Hawaii, 1000 Pope Road, MSB, Honolulu, HI 96822.

A. Soloviev, Oceanographic Center, Nova Southeastern University, 8000 North Ocean Drive, Dania Beach, FL 33004. (e-mail: soloviev@ocean.nova.edu)